Tracking Forearm Motor Units Across Constrained and Unconstrained Finger Force Control Tasks

Jan Bodenschlägel
Chair of Digital Health & Data Science
University of Bayreuth
Bayreuth, Germany
jan.bodenschlaegel@uni-bayreuth.de

Renato Mio
Chair of Digital Health & Data Science
University of Bayreuth
Bayreuth, Germany
renato.mio-zaldivar@uni-bayreuth.de

A. Aldo Faisal
Chair of Digital Health & Data Science
University of Bayreuth
Bayreuth, Germany
Brain & Behaviour Lab
Imperial College London
London, United Kingdom
aldo.faisal@uni-bayreuth.de

***Abstract*—Reliable motor unit (MU) tracking across varied finger force conditions is crucial for neural interfaces that must function beyond controlled laboratory settings. We investigated whether individual MUs can be tracked between constrained force tasks and naturalistic finger force patterns using high-density surface EMG. Twenty-five participants performed isometric flexion of thumb, index, and middle fingers at 10 % and 20 % of maximum voluntary force, plus unconstrained multi-finger tasks, while recording multichannel EMG from the anterior forearm muscles. MU decomposition identified 302 ± 90 MUs per participant, with recruitment increasing 45-70% when force doubled. Spatial activation patterns matched anatomical expectations: thumb MUs were localised radially; index/middle finger MUs, ulnarly. Notably, 96.7 % of MUs could be tracked across different trials of the same or different conditions at correlation threshold 0.7, with 62.8 % remaining trackable at 0.9 threshold. More MUs were shared between index and middle finger tasks than with thumb tasks, reflecting anatomical organization. Cross-condition tracking was highly dependent on the correlation threshold, with 0.9 required for reliable individual MU identification. These findings show that subject-specific MU patterns can be tracked across controlled and naturalistic conditions, which is crucial for future MU-based neural interfaces in real-world applications.**

***Index Terms*—high-density EMG, motor units, isometric contraction, neural signal processing**

I. Introduction

Surface electromyography (EMG) of hand and finger movements enables intuitive neural interfacing with assistive devices that enhance mobility in daily life [1]–[3]. Muscle contractions are driven by the motor cortex [5], [6], which sends electrochemical signals through the spinal cord to motor units (MUs) — muscle fibers activated by α-motor neurons. These motor unit action potentials (MUAPs) trigger muscle movement, and their combined activity at a site forms the EMG signal [7]. Although EMG recording and processing are now straightforward [8], interpretation remains complex. Current approaches include classifying EMG using statistical or neural network methods [9]–[11] or decomposing signals into MU spike trains [3], [4], [12].

MU decomposition over multichannel EMG signals applies blind source separation techniques, often based on independent component analysis (ICA), to extract individual MUs spiking discharge times [13], [14]. This also enables the characterisation of MUs by their force-dependent recruitment threshold [15], [17], [18]. Moreover, the output of the algorithm can also be used to compute MUAP waveforms across all EMG channels by spike-triggered averaging. Spatial distribution and waveform shapes of MUAPs can then be used to track MU activity across different tasks using a method called MU tracking [12], [18], [19].

Previous studies focused on tracking MUs in large leg muscles (e.g. the tibialis anterior) where MUs can be more easily and reliably decoded due to their anatomical properties. One application was to analyse muscles contractions with varying strength across sessions to explore how training affects MU activity [19], [20]. More recent work applies MU tracking to finger movements, linking MUs to changes in finger position [12] or exerted force [21]. In all these cases, MUs are tracked across mostly controlled tasks, where muscle force is isometric and maintained at a constant level most of the time.

To explore the feasibility of MU tracking between constrained and more naturalistic conditions, we investigated whether MUs decoded from forearm muscles during constrained finger force tasks can be tracked into different constrained and unconstrained tasks. We recorded multichannel EMG signals from the forearm during isometric flexion of the thumb, index, and middle fingers using a custom finger force-measuring device. The goal of this study was to analyse MU activity in relation to applied force, using MU tracking to identify patterns and differences in MU behaviour during constant versus unconstrained finger force application.

II. Material and methods

A. Experimental setup

For the recording of finger forces, a custom measurement device, akin to a vertical computer mouse, was designed

This work is supported by the Hightech-Agenda Bavaria. AAF acknowledges support from the United Kingdom Research and Innovation Turing AI Fellowship (EP/V025449/1).

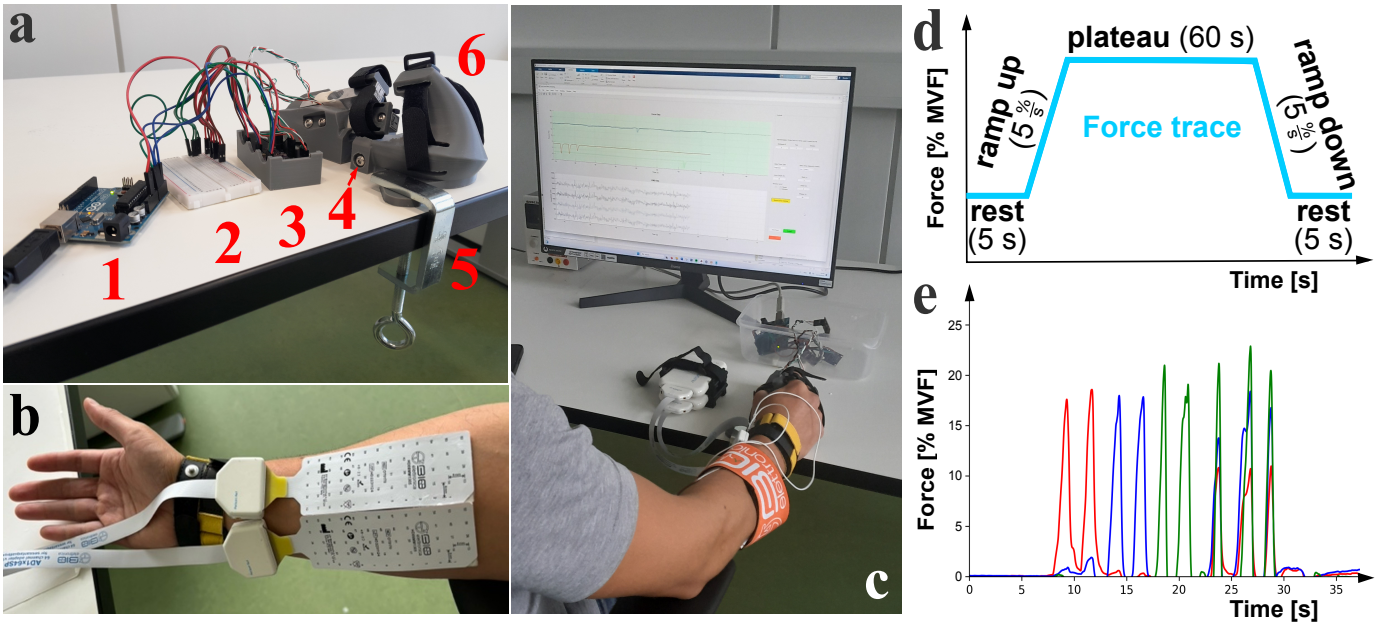

Fig. 1. (**a**) Custom finger force recording handheld device consisting of (1) Arduino Uno R3 (2) Protoboard (3) Case with CJMCU-711 A/D converters (4) Size adjustment (5) C-clamp fixation (6) Case with embedded load cells (**b**) Two applied 64-channel rectangle electrode grids on the forearm (**c**) Experimental setup: The participant sits in front of a monitor displaying the force trace during application of finger force to the computer mouse-like device. A few EMG channels' signals are also displayed in real-time (**d**) Trapezium force trace used in constant force trials (**e**) Example trial from unconstrained force condition. The pattern is volitionally chosen by the participant.

on Autodesk Inventor (Version 2024, Autodesk, San Francisco, USA) and then 3D-printed (AnyCubic Kobra, Anycubic, Shenzhen, China) using polyactic acid filament (Fig. 1**a**). The device was fitted with load cells for the 10 kg range, which allows recording within the typical maximum isometric pinch forces of the targeted fingers (72.8 ± 23.4 N for the thumb; 42.6 ± 12.5 N for the index; 39.0 ± 7.6 N and 50.0 ± 9.7 N for the middle finger of men and women, respectively [22], [23]). The output of the load cells was converted using a CJMCU-711 24-bit analog-digital converter and sent to an Arduino Uno R3 (Arduino, Strambino, Italy). Force data were sampled at 50 Hz and sent from Arduino to the PC via serial communication. Versions were created for both left- and right-handed users, with adjustable sizing for the hand. EMG signals were recorded over the anterior forearm with two 64-channel electrode grids (13x5 electrodes, 8 mm inter-electrode distance, HD08MM1305, OT Bioelettronica, Turin, Italy, Fig. 1**b**) at a sampling frequency of 2000 Hz using two wireless analog-to-digital converters (Sessanataquattro+, OT Bioelettronica, Turin, Italy) and a SyncStation (OT Bioelettronica, Turin, Italy). The anterior forearm was shaved, cleaned and prepared with a abrasive skin preparation gel. EMG electrode grids were applied using adhesive foam layer (FOA08MM1305, OT Bioelettronica, Turin, Italy) with a conductive paste. To ensure better skin contact with the electrodes, the electrode grids were additionally fixed to the forearm with bandages.

B. Protocol

The experimental protocol began with the removal of all electronic devices, collection of personal data, assessment of handedness using the Edinburgh Handedness Inventory, and measurement of maximum grip force of the dominant hand using a PowerLab 26T (Model PL26T04, ADInstruments, Dunedin, New Zealand; sampling rate: 5 Hz).

Force measurements were calibrated to each participant's maximum voluntary force (MVF) for each finger of the dominant hand to enable cross-subject comparisons. Prior to the recording, the maximum force for each finger was used to normalise forces applied during individual trials.

EMG signals and forces from the thumb, index, and middle fingers of the dominant hand were recorded at constant force levels of 10 % and 20 % MVF. A MatLab (Version R2024b, The MathWorks, Natick, USA) script displayed the target force on a monitor (Fig. 1**c**) using a trapezoidal profile consisting of 5 s rest, 5 %MVF/s force ramp-up to the target 60-second plateau, and then 5 %/s ramp-down, ending with 5 s rest (Fig. 1**d**). Additional 20 s trials involved unconstrained force application by one to three fingers for more realistic data (Fig. 1**e**). Each finger underwent five trials at 10 % and 20 % MVF, followed by five unconstrained trials.

C. Data collection

Data were collected from 25 healthy adult subjects (age: 28.8 ± 7.7 years; 15 female; 22 right-handed; max grip force: 372.7 ± 128.6 N; Body-Mass-Index: 25.1 ± 5.7 kg/m^2) with no reported neuromotor disorders. All participants gave informed and voluntary written consent. The study was approved by the University of Bayreuth ethics committee (Application No. 24-030).

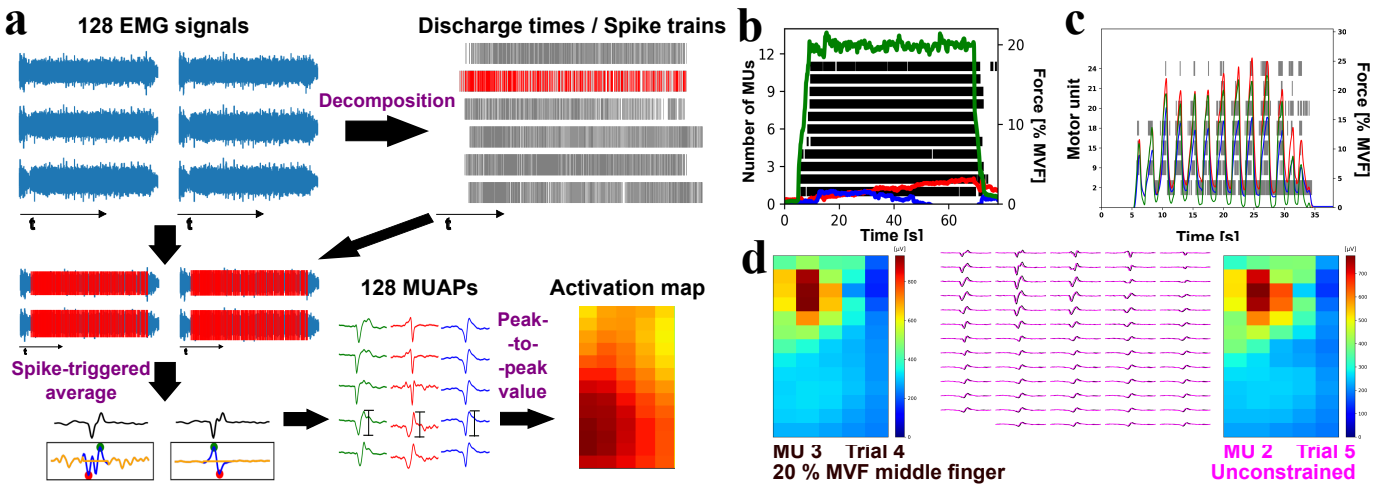

Fig. 2. (**a**) EMG data processing pipeline: After decomposition into MU discharge times/spike trains, superimposition of the EMG data is achieved by calculating the spike-triggered average to get MUAP waveforms (black) per recorded EMG channel (left box: rejected by filter, right box: accepted, green dot: global maximum, red dot: global minimum, blue: signal curve, yellow: noise curve); assigning the peak-to-peak values to the placement of the EMG channels creates an activation map (**b**) Spike trains and force curves of thumb (red), index finger (blue) and middle finger (green) after decomposition of a constrained force trial at 20 % MVF of the middle finger (**c**) unconstrained force trial of multiple finger force application of thumb (red), index finger (blue), and middle finger (green) with corresponding filtered MUs marked by its number and their spike trains (gray) (**d**) Visualisation of MU tracking applied to MU 3 from trial 4 of the middle finger at a constant force of 20 % MVF (left: activation map, middle: MUAP waveforms in black) with MU 2 of the trial 5 in unconstrained force condition (right: activation map, middle: MUAP waveforms in magenta), from participant 15.

D. Signal Processing

The EMG signals were preprocessed with a Notch filter to suppress 50 Hz power line noise and its harmonic frequencies, and a bandpass filter from 20 - 500 Hz for the neuronal signals [7]. Electrode channels were visually inspected and noisy or flat channels (6.5 ± 4.3 per trial) were removed. MU spike trains were obtained from the multichannel EMG data using the blind source separation algorithm for MU decomposition from Negro et al. with 100 iterations and a 0.7 silhouette threshold [14]. Briefly, a fixed-point iteration procedure can be used to obtain separation vectors which convert the multichannel EMG into a variable number of individual MUs. As MU firings are inherently sparse over time, the aim of the algorithm is to maximise the sparsity of the detected sources (i.e. the MUs), thus extracting the sparse spike trains of individual MUs from complex, overlapping EMG signals. The algorithm was applied to each electrode grid separately, and then duplicate MUs were removed. Two spike trains are considered duplicates of the same MU when the number of common spikes (i.e. with same discharge timings) between them exceeds 30% of the total number of spikes in the MU with more spikes. The spike train with lower coefficient of variation (CoV) of inter-spike intervals (ISI) is the one kept. For each MU, spike-triggered averaging over the multichannel EMG time series determined the MUAP waveforms and their peak-to-peak values (Fig. 2**a**) [15].

E. Motor unit filtering

In addition, we analysed and discarded low-quality or physiologically implausible MUs applying several criteria. First, we removed MUs with tonic behaviour (active throughout the whole trial) or with activity outside the force-active segments of the trace. In the constrained trials, we also removed MUs active 5 s prior to force application. To further filter out implausible MUs, we also removed MUs with mean firing rates below 5 spikes/s [16]. Additionally, we removed MUs with low MUAP waveform amplitudes (peak-to-peak values) relative to others in the trial. This implied computing the mean signal-to-noise ratio (SNR) of all MUAP waveforms per MU and discarding the MU if that SNR was less than 5 dB. MUs with physiologically implausible MUAP waveforms were determined by counting the peaks and valleys in the waveform. If this number exceeded four, an overlap of two or more MUs was assumed and the MU was removed. As illustrated in Fig. 2**a**, examples of a removed MU and a retained MU are displayed in boxes.

Filtered MU spike trains for constrained and unconstrained force are shown in (Fig. 2**b**) and (Fig. 2**c**). The number of filtered MUs was statistically analysed, and as the data was not normally distributed (Shapiro-Wilk test, $p < 0.05$), differences were assessed using the Wilcoxon signed rank test. Activation maps were created from the filtered MUs to visualise their spatial distribution [24], with missing values replaced by median values from neighbouring channels.

F. Motor unit tracking

To track MUs across trials, the activation maps and MUAP waveforms of filtered MUs were analysed (Fig. 2**d**). First, pairwise correlations between activation maps were calculated using Spearman's rank-order correlation coefficient, as the data were not normally distributed (Shapiro-Wilk test, $p < 0.05$). Correlations were considered significant if the Spearman coefficient met or exceeded a predefined threshold. Spearman rank-order coefficients allowed comparison of MU positions

regardless of linearity. Next, MUAP waveforms were compared via cross-correlation of waveforms recorded from the same channels across different trials. The maximum cross-correlation value was normalised to the signal magnitudes, and if the mean of all normalised cross-correlations exceeded the threshold, the MU correlation was accepted. Correlation thresholds of 0.7, 0.8, and 0.9 were applied.

This tracking procedure was used to identify common MUs across all trials for each subject. The ratio of tracked MUs was calculated by dividing the number of matching MUs across trials by the total number of filtered MUs in each trial condition. This was repeated for each correlation threshold.

III. Results

A. Decomposed and filtered motor units

Across all trials, the total number of filtered decoded MUs was 302.4 ± 89.7 per subject. The number of filtered MUs per trial at constrained conditions for thumb, index, and middle finger at 10 % MVF were 5.5 ± 3.8, 6.7 ± 5.1, 7.1 ± 4.8; at 20 % MVF 7.7 ± 4.1, 9.6 ± 5.9, and 11.3 ± 6.2. Fig. 3 shows a box plot of the average number of filtered MUs per trial across conditions.

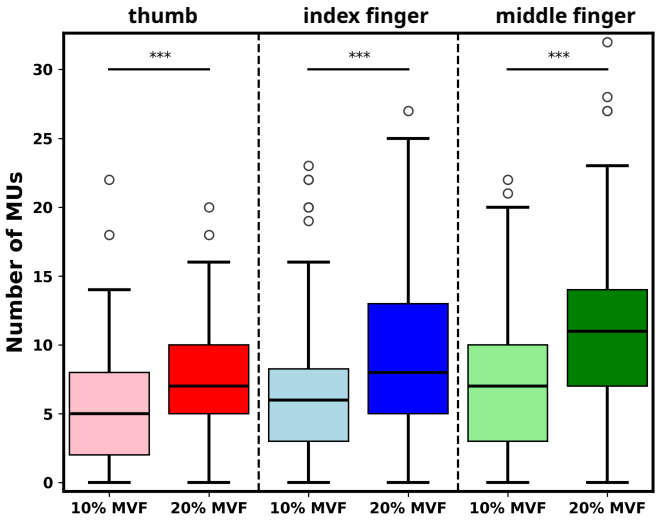

Fig. 3. Number of filtered MUs resolved for each trial of constrained force application at 10 and 20 % maximum voluntary force (MVF) of the thumb (red), index finger (blue) and middle finger (green), Mean values marked with (***) differed significantly with a p-value < 0.001.

Our filtered MU counts per condition are comparable to those reported in previous studies [12], [21]. More MUs are recruited at higher force levels. The number of filtered MUs per trial for individual finger flexions differs significantly between 10 % and 20 % MVF per digit (p-value < 0.001).

In unconstrained force trials, an average of number of 67.2 ± 38.9 MUs were resolved per trial, with 13.9 ± 6.9 MUs after filtering. MU counts varied widely since only a 20 % MVF maximum force limit was set. Unlike constant force trials, continuously active MUs were retained, and multiple finger movements could occur simultaneously, resulting in a higher total MU count.

B. Activation maps from constrained force trials

The activation maps of each grid were summarised from the filtered MUs of the constrained trials and the mean value per MU is shown in Fig. 4. The shown maximum peak-to-peak value of average MU is higher at 20 % MVF than at 10 %. A more detailed analysis of the average maximum peak-to-peak values for each finger reveals increases of 45.5 % for the thumb, 69.7 % for the index finger, and 58.3 % for the middle finger, at 20 % MVF application compared to 10 % MVF.

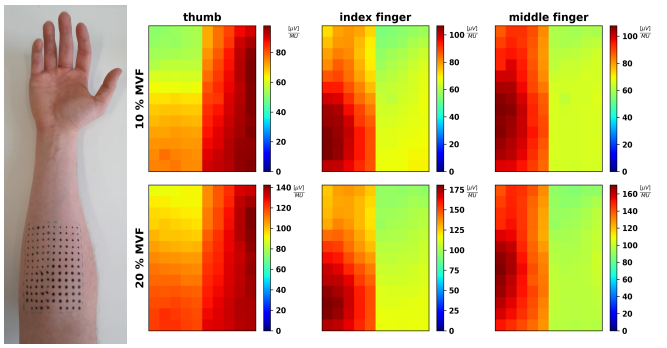

Fig. 4. Left: Recording area on the proximal forearm with black dots showcasing electrode positions. Right: Activation maps over the two 64-channel grids during constrained force trials of the thumb, index, and middle finger, at 10 % MVF (top) and 20 % MVF (bottom).

Active MU areas differ by finger. During thumb flexion, activation is mainly radial, while index and middle finger flexion show ulnar activation, reflecting the anatomical structure: the thumb is controlled by the radial *flexor pollicis longus*, and the index and middle fingers by the ulnar *flexor digitorum profundus* [25]. Additionally, index finger flexion is associated with more proximal MU activation than that of the middle finger.

C. Motor unit tracking

To track MUs across trials, activation maps and MUAP waveforms of MUs from different trials were compared. The average number of tracked MUs and the average ratio to the maximum MU count of a single subject are shown in Table I.

As shown in Table I, more MUs are tracked at lower correlation thresholds. At a threshold of 0.7, nearly all MUs are tracked in at least one other trial. Even at 0.9, 62.77 % of MUs are still matched per subject, indicating reliable tracking across trials. The sharp rise in tracked MUs at lower thresholds might be due to overlapping activation areas, where a single

TABLE I
Number of tracked MUs at different correlation thresholds

Correlation threshold	0.7	0.8	0.9
Tracked MUs per subject	292.1 ± 93.1	264.7 ± 89.2	180.3 ± 72.1
Compared to all MUs [%]	96.72 ± 2.23	89.57 ± 3.50	62.77 ± 10.57

MU may be linked to multiple others rather than forming distinct one-to-one matches.

Fig. 5 provides a detailed overview of MU tracking across conditions based on the correlation threshold. Each cell shows the number of MUs decoded from one condition (columns) and tracked to another condition (rows). For example, at a correlation threshold of 0.7, 362 MUs decoded in 10 % MVF thumb flexion trials (52.92 % of all MUs for that condition) were tracked into 10 % MVF index finger flexion trials. Several MUs are shown to be tracked across all conditions and correlation thresholds. The matrices are not symmetrical, as there are five trials per condition and the MUs are also matched with multiple others within the same condition.

Most tracked MUs are found in constrained trials involving the same finger, especially at the higher correlation threshold of 0.9. Additionally, more MUs are tracked between index and middle finger trials than between the thumb and either finger. These patterns reflect the spatial distribution of MU activity, as shown in Section III-B. Activation areas are similar when the same finger applies different force levels, and also between the index and middle fingers. In contrast, the MU activation areas during thumb flexion differ significantly, leading to fewer shared MUs with the other fingers.

When comparing constrained and unconstrained conditions, more MUs are tracked between the index and middle fingers than between the thumb and either finger. This could be due to the lower number of decoded and filtered MUs in thumb trials compared to the index and middle fingers. Similarly, fewer MUs were tracked at lower force levels, as fewer MUs were identified under these conditions.

Fig. 5 demonstrates that higher correlation thresholds yield more accurate MU tracking, prompting the question of whether individual MUs can be reliably assigned to specific finger movements. Table II presents the average number of MUs tracked from constrained trials into same-digit tasks, into different-digit tasks, or into unconstrained conditions per subject. It also indicates whether these MUs were tracked exclusively within those specific conditions. As previously observed, more MUs are tracked in trials involving the same finger than across different fingers, with a higher proportion

TABLE II
TRACKED MUS FROM EVERY DIGIT INTO SAME-DIGIT TRIALS, INTO DIFFERENT-DIGIT TRIALS, AND INTO UNCONSTRAINED TRIALS

	Digit		
	Thumb	Index	Middle
Initial MU pool per digit	65.3 ± 27.7	87.8 ± 39.1	104.9 ± 41.9
Tracked into same digit only	22.0 ± 15.5	16.6 ± 13.2	27.2 ± 22.1
Tracked into same and different digits	20.08 ± 22.9	33.4 ± 25.7	36.6 ± 25.6
Tracked into different digits only	5.8 ± 8.3	8.4 ± 9.1	6.0 ± 5.9
Tracked into unconstrained trials	10.6 ± 12.1	19.2 ± 19.0	56.2 ± 80.3

*Results at 0.9 matching correlation threshold

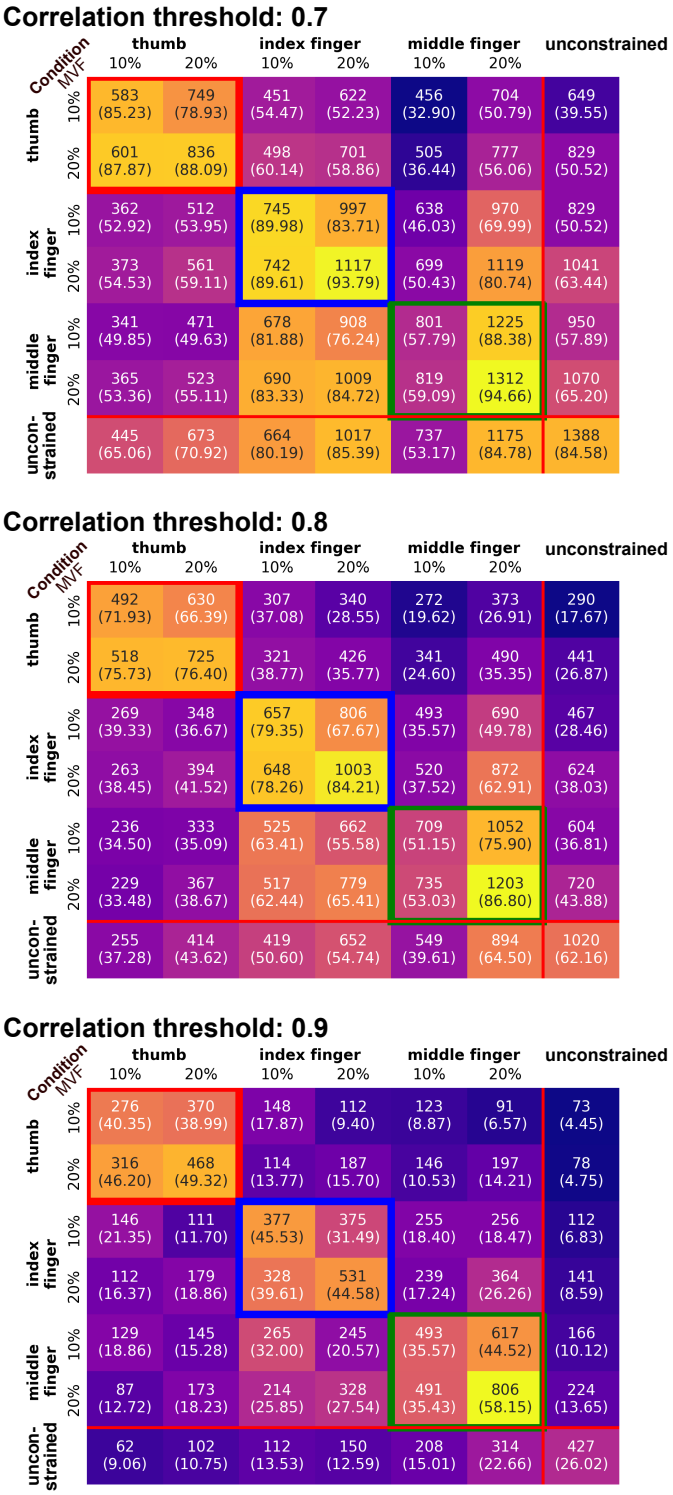

Fig. 5. Number of tracked MUs and percentages (in brackets) relative to the total number of MUs in each condition (digit and force level combination, or unconstrained). MU counts come from all subjects with MU tracking applied between all trials with different conditions. Different thresholds for the correlation of activation maps and cross correlation of MUAP waveforms were tested: 0.7 (top), 0.8 (middle), 0.9 (bottom). Columns correspond to the conditions in which MUs were initially decoded and rows correspond to the condition into which they were tracked. Constrained and unconstrained trial conditions are separated by red horizontal and vertical lines. Coloured rectangles frame same-digit conditions (thumb: red, index finger: blue, middle finger: green)

dedicated to individual finger movements. High standard deviations reflect participant-specific variability in the number of resolved MUs, especially in unconstrained tasks. Tracking across different fingers yields fewer MUs, with very few being task-specific. This indicates that while many MUs are uniquely involved in single-finger movements, only some contribute to only multiple-digit actions. To more precisely assign MUs to specific force levels and finger movements, it is necessary to conduct more extensive experiments involving both single- and multi-digit tasks.

IV. Conclusion

This study shows the feasibility of reliable MU tracking across constrained and unconstrained finger force tasks, achieving 96.7% tracking success at correlation threshold 0.7 and 62.8% at the stringent 0.9 threshold. Reliable individual MU identification requires high correlation thresholds, creating a trade-off between detection sensitivity and identification specificity.

MU recruitment increased predictably with force (45-70% when doubling from 10% to 20% MVF), and spatial activation patterns aligned with anatomical expectations: radial activation for thumb flexion, ulnar for index and middle fingers. Greater MU overlap occurred between index and middle finger tasks than with thumb combinations, reflecting shared neural control mechanisms. However, substantial individual variability, particularly in unconstrained conditions, indicates that subject-specific calibration will be essential for robust implementations.

This work provides a baseline for subject-specific MU-based neural interfaces capable of functioning in naturalistic movement scenarios by reporting quantitative results in MU tracking beyond controlled force traces. However, the correlation threshold dependency and individual differences highlight the need for personalised approaches. Future work should validate these methodologies in real-time applications and develop adaptive algorithms to optimise the robustness of MU tracking in naturalistic manipulation scenarios.

References

[1] M. Xiloyannis, Constantinos Gavriel, Andreas, and A. A. Faisal, "Dynamic forward prediction for prosthetic hand control by integration of EMG, MMG and kinematic signals," vol. 26, pp. 611–614, Apr. 2015.

[2] J. Eden et al., "Principles of human movement augmentation and the challenges in making it a reality," Nature Communications, vol. 13, no. 1, Mar. 2022.

[3] D. S. Oliveira et al., "A direct spinal cord–computer interface enables the control of the paralysed hand in spinal cord injury," Brain, Mar. 2024.

[4] R. Mio, J. Narayan, and A. A. Faisal, "Motor Unit Decomposition Over Intrinsic Hand Muscles During Single and Multi-finger Flexion," Biosystems & biorobotics, pp. 115–119, Jan. 2025.

[5] S. C. Cramer, S. P. Finklestein, J. D. Schaechter, G. Bush, and B. R. Rosen, "Activation of Distinct Motor Cortex Regions During Ipsilateral and Contralateral Finger Movements," Journal of Neurophysiology, vol. 81, no. 1, pp. 383–387, Jan. 1999.

[6] G. Hotson et al., "Individual Finger Control of the Modular Prosthetic Limb using High-Density Electrocorticography in a Human Subject," Journal of neural engineering, vol. 13, no. 2, p. 026017, Apr. 2016.

[7] R. Merletti and S. Muceli, "Tutorial. Surface EMG detection in space and time: Best practices," Journal of Electromyography and Kinesiology, vol. 49, p. 102363, Dec. 2019.

[8] H. Tankisi, "Standards of instrumentation of EMG," Clinical Neurophysiology, vol. 131, no. 1, pp. 243–258, Jan. 2020.

[9] A. Moin et al., "A wearable biosensing system with in-sensor adaptive machine learning for hand gesture recognition," Nature Electronics, vol. 4, no. 1, pp. 54–63, Dec. 2020.

[10] A. Toro-Ossaba, J. Jaramillo-Tigreros, J. C. Tejada, A. Peña, A. López-González, and R. A. Castanho, "LSTM Recurrent Neural Network for Hand Gesture Recognition Using EMG Signals," Applied Sciences, vol. 12, no. 19, p. 9700, Jan. 2022.

[11] G. Gu, N. Zhang, C. Chen, H. Xu, and X. Zhu, "Soft Robotics Enables Neuroprosthetic Hand Design," ACS Nano, vol. 17, no. 11, pp. 9661–9672, May 2023.

[12] M. Osswald, A. L. Cakici, D. Souza, D. I. Braun, D. Farina, and A. D. Vecchio, "Task-Specific Motor Units in the Extrinsic Hand Muscles Control Single- and Multi-Digit Tasks of the Human Hand," Journal of Applied Physiology, Apr. 2025.

[13] A. Holobar, M. A. Minetto, and D. Farina, "Accurate identification of motor unit discharge patterns from high-density surface EMG and validation with a novel signal-based performance metric," Journal of Neural Engineering, vol. 11, no. 1, p. 016008, Jan. 2014.

[14] F. Negro, S. Muceli, A. M. Castronovo, A. Holobar, and D. Farina, "Multi-channel intramuscular and surface EMG decomposition by convolutive blind source separation," Journal of Neural Engineering, vol. 13, no. 2, p. 026027, Feb. 2016.

[15] J. Rodriguez-Falces, F. Negro, M. Gonzalez-Izal, and D. Farina, "Spatial distribution of surface action potentials generated by individual motor units in the human biceps brachii muscle," Journal of Electromyography and Kinesiology, vol. 23, no. 4, pp. 766–777, Aug. 2013.

[16] A. W. Monster and H. Chan, "Isometric force production by motor units of extensor digitorum communis muscle in man," Journal of Neurophysiology, vol. 40, no. 6, pp. 1432–1443, Nov. 1977.

[17] A. Del Vecchio, A. Holobar, D. Falla, F. Felici, R. M. Enoka, and D. Farina, "Tutorial: Analysis of motor unit discharge characteristics from high-density surface EMG signals," Journal of Electromyography and Kinesiology, vol. 53, p. 102426, Aug. 2020.

[18] G. Valli, P. Ritsche, A. Casolo, F. Negro, and Giuseppe De Vito, "Tutorial: Analysis of central and peripheral motor unit properties from decomposed high-density surface EMG signals with openhdemg," Journal of electromyography and kinesiology, vol. 74, pp. 102850–102850, Feb. 2024.

[19] E. Martinez-Valdes, F. Negro, C. M. Laine, D. Falla, F. Mayer, and D. Farina, "Tracking motor units longitudinally across experimental sessions with high-density surface electromyography," The Journal of Physiology, vol. 595, no. 5, pp. 1479–1496, Feb. 2017.

[20] A. Del Vecchio et al., "The increase in muscle force after 4 weeks of strength training is mediated by adaptations in motor unit recruitment and rate coding," The Journal of Physiology, vol. 597, no. 7, pp. 1873–1887, Feb. 2019.

[21] Y. Li, Y. Zheng, G. Xu, S. Zhang, R. Liang, and R. Ji, "Classification of Action Potentials With High Variability Using Convolutional Neural Network for Motor Unit Tracking," IEEE Transactions on Neural Systems and Rehabilitation Engineering, vol. 32, pp. 905–914, Jan. 2024.

[22] Kinoshita, H., Murase, T., and Bandou, T., "Grip posture and forces during holding cylindrical objects with circular grips," Ergonomics, vol. 39, no. 9, pp. 1163–1176, Sep. 1996.

[23] Li, YX., Lv, N., Zhao, Y. et al., "Contributions of the thumb and index finger to tip pinch force sense," Science Reports, vol. 15, no 23687, Jul. 2025.

[24] R. Merletti, A. Holobar, and D. Farina, "Analysis of motor units with high-density surface electromyography," Journal of Electromyography and Kinesiology, vol. 18, no. 6, pp. 879–890, Dec. 2008, doi: https://doi.org/10.1016/j.jelekin.2008.09.002.

[25] Ebubechi Okwumabua, M. A. Sinkler, and B. Bordoni, "Anatomy, Shoulder and Upper Limb, Hand Muscles," Nih.gov, Jul. 24, 2023. https://www.ncbi.nlm.nih.gov/books/NBK537229/?report=reader#_NBK537229_pubdet_ (accessed May 19, 2025).